Water Research 160 (2019) 238–248

Contents lists available at ScienceDirect

Water Research

journal homepage: www.elsevier.com/locate/watres

Degradation of naphthalene with magnetic bio-char activate hydrogen peroxide: Synergism of bio-char and Fe–Mn binary oxides

Ling Li [a, b], Cui Lai [a, b, *], Fanglong Huang [a, b], Min Cheng [a, b, **], Guangming Zeng [a, b], Danlian Huang [a, b], Bisheng Li [a, b], Shiyu Liu [a, b], MingMing Zhang [a, b], Lei Qin [a, b], Minfang Li [a, b], Jiangfan He [a, b], Yujin Zhang [a, b], Liang Chen [c]

[a] College of Environmental Science and Engineering, Hunan University, Changsha, Hunan, 410082, China
[b] Key Laboratory of Environmental Biology and Pollution Control (Hunan University), Ministry of Education, Changsha, Hunan, 410082, China
[c] Faculty of Life Science and Technology, Central South University of Forestry and Technology, Changsha, Hunan, 410004, China

ARTICLE INFO

Article history:
Received 25 December 2018
Received in revised form
16 May 2019
Accepted 25 May 2019
Available online 26 May 2019

Keywords:
Fe-Mn modification
Bio-char
Naphthalene
Hydrogen peroxide
Hydroxyl radicals

ABSTRACT

This study investigated the hydrogen peroxide (H_2O_2) activation potential of Fe–Mn binary oxides modified bio-char (FeMn/bio-char) for the degradation of naphthalene, the dominant PAHs in drinking water. Results showed that FeMn/bio-char exhibited 80.7- and 2.18-times decomposition rates towards H_2O_2 than that of pure bio-char and Fe–Mn binary oxides, respectively, and consequently the FeMn/bio-char/H_2O_2 photo-Fenton system presented highest naphthalene removal efficiency. The enhanced catalytic activity could be ascribed to the synergistic effect of the combination of bio-char and Fe–Mn binary oxides, such as promoting the adsorption capacity towards contaminant, increasing concentration of persistent free radicals (PFRs) and introducing Fe–Mn binary oxides as new activator. According to the batch-scale experiments, FeMn/bio-char/H_2O_2 photo-Fenton system could degrade naphthalene effectively at a wide pH ranges, and 82.2% of naphthalene was degraded under natural pH of 5.6 within 148 min. Free radicals quenching studies and electron spin resonance (ESR) analyses verified that the dominant free radical within FeMn/bio-char/H_2O_2 photo-Fenton system was hydroxyl radical (•OH). According to the preliminary analysis, the generation of •OH were ascribed to the activation of H_2O_2 by Fe (II), Mn (II) and PFRs on the catalyst surface. The mainly degradation intermediates of naphthalene were identified by GC-MS analysis. Consequently, the possible degradation pathways were proposed. Moreover, naphthalene degradation experiments were also conducted in river, tap water, industrial wastewater as well as medical wastewater, and the results indicated that the FeMn/bio-char/H_2O_2 photo-Fenton system was effective in the treatment of naphthalene in natural waters. This study brings a valuable insight for the potential environmental applications of modified bio-char.

1. Introduction

Nowadays, the rapid expansion of industrial scale and population has resulted in the discharging of various natural and synthetic refractory aromatic organic contaminants to the natural water systems, which have potential adverse effects towards aquatic ecology and human health (Lai et al., 2016; Zhou et al., 2018; Yi et al., 2019). Among the environmental issues, polycyclic aromatic hydrocarbons (PAHs) pollution has drawn attention in recent years because of the toxicity, mutagenicity and carcinogenicity of PAHs (Liu et al., 2017). Additionally, PAHs are an important class of persistent organic pollutants (POPs), which can persistently present in environment due to their stability and strong recalcitrant nature (Sekar et al., 2018). Table S4 present the typical concentration of PAHs in actual water. Thus, developing an effective method for PAHs degradation is necessary and important.

Advanced oxidation processes (AOPs) have been recognized as promising technologies for the degradation of many hazardous and biorefractory contaminants (Li et al., 2018; Lai et al., 2019a; Qin et al., 2019). Among these AOPs, hydroxyl radical (•OH) generated from Fenton process has received particular attention (Cheng et al., 2018a). •OH has a redox potential of 2.8 V, which can react non-selectively with organic pollutants and completely decompose

* Corresponding author. College of Environmental Science and Engineering, Hunan University, Changsha, Hunan, 410082, China.
** Corresponding author. College of Environmental Science and Engineering, Hunan University, Changsha, Hunan, 410082, China.
E-mail addresses: laicui@hnu.edu.cn (C. Lai), Chengmin@hnu.edu.cn (M. Cheng).

https://doi.org/10.1016/j.watres.2019.05.081
0043-1354/

them into CO_2, H_2O and inorganic salts with rate constants of 10^6–10^9 M^{-1} s^{-1} (Cheng et al., 2019). Hydrogen peroxide (H_2O_2) has been widely used as an oxidant for the generation of •OH. Up till now, activation of H_2O_2 has been reported by several pathways such as direct photolysis of H_2O_2 (An and Carraway, 2002) and Fenton/Fenton-like oxidation (Lai et al., 2019b).

Bio-char is a low-cost and carbon-rich porous substance produced by pyrolysis of various waste biomass (Zhang et al., 2019; Wu et al., 2017). Considering cost and solid waste reuse, bio-char is regarded as a promising alternative heterogeneous catalyst for wastewater treatment. In addition to adsorption capacity, recent studies indicated that bio-char is also capable of catalyzing H_2O_2 because of persistent free radicals (PFRs) (Fang et al., 2015; Qin et al., 2018). The PFRs existed on the bio-char surface may activate H_2O_2 decomposition to form •OH and further degrade organic pollutants in water. For example, Fang et al. (2014) have reported that heterogeneous catalytic oxidation by H_2O_2 coupled with bio-char showed efficient decontamination of 2-chlorobiphenyl, among which PFRs was found to be a great activator. However, the performance of bio-char fails to meet the requirement of actual applications since the PFRs concentration of bio-char markedly decreased after activating H_2O_2 (Fang et al., 2014; Qin et al., 2018), and bio-char are inconvenient to recycle from the treated effluent for reuse.

It is an interesting issue to improve the catalytic performance of bio-char in real wastewater treatment, of various activating technologies, modified bio-char with Fe–Mn binary oxides might be an effective solution. Fe and Mn elements are widely existing in the steel slag and metallurgical wastewater. Moreover, Fe–Mn binary oxides are kinds of Fenton-like catalysts which exhibit better stability in catalyzing H_2O_2 (Wan and Wang, 2017a; Wang et al., 2018). Nevertheless, magnetic Fe–Mn binary oxides tend to aggregate which may influence its catalytic activity. Different approaches, such as dispersing transitional metal oxides onto carbon materials (Ouyang et al., 2017) or using fluidized-bed Fenton (FBF) reactors (Garcia-Segura et al., 2016) can avoid catalyst agglomeration. Combination of bio-char with Fe–Mn binary oxides are presumed to achieve the following synergistic effects in enhancing the oxidization of the H_2O_2 system: (I) Fe–Mn binary oxides attached on bio-char can act as a new activator of H_2O_2; (II) metal treatment can increase the concentration of PFRs in bio-char (Fang et al., 2015); (III) the catalyst can be separated by external magnetic fields owing to the magnetic property of Fe–Mn binary oxides (Liu et al., 2019). Simultaneously, bio-char can prevent the aggregation of Fe–Mn binary oxides. Thus, designing a binary heterogeneous catalyst of bio-char and Fe–Mn binary oxides and then making it combine with H_2O_2 to form a heterogeneous Fenton-like system seems to be very attractive.

In this study, Fe–Mn binary oxides modified bio-char (FeMn/bio-char) was fabricated via one-step pyrolysis method. In addition, numerous studies have reported that the introduction of visible light into Fenton process can enhance the catalytic capacity towards H_2O_2 due to the regeneration of Fe^{2+} (Babuponnusami and Muthukumar 2014). Hence visible light irradiation was introduced into this FeMn/bio-char/H_2O_2 Fenton-like system to promote the catalytic activity of catalyst. Naphthalene, the dominant PAHs in drinking water (Lair et al., 2008), was selected as a model compound to investigate the removal of PAHs from the contaminated aquatic systems.

The purposes of this study were to (1) produce a novel photo-Fenton system based on FeMn/bio-char; (2) investigate the effects of different experimental parameters on the degradation performance of naphthalene, such as H_2O_2 concentration, catalyst dosage and initial pH; (3) clarify the activation mechanism of H_2O_2 by FeMn/bio-char and explore the synergistic promoting effect between bio-char and Fe–Mn binary oxides; (4) propose the possible degradation intermediates and reaction pathway of naphthalene.

2. Materials and methods

2.1. Materials

Manganese dichloride tetrahydrate ($MnCl_2 \cdot 4H_2O$), Ferric chloride hexahydrate ($FeCl_3 \cdot 6H_2O$) and hydrogen peroxide (H_2O_2) were obtained from Sinopharm Chemical Reagent Corp (Beijing, China). Naphthalene was purchased from Aladdin Industrial Corporation (Shanghai, China). The chemicals used in this work were of analytical grade. Ultrapure water with a resistivity of 18.25 MΩ was used for the preparation of aqueous solutions.

2.2. Preparation of catalysts

Pine needles were collected from Changsha of Hunan province, China. After being washed by ultrapure water several times, pine needles were dried at 105 °C for 24 h and grinded by a cutting mill, then passed through a 100-mesh sieve. The raw pine needles particles were retained and used as feedstock for impregnation.

The FeMn/bio-char samples were synthesized through wet impregnation method with one-step pyrolysis, using $FeCl_3 \cdot 6H_2O$ as iron source and $MnCl_2 \cdot 4H_2O$ as manganese source. The preparation process is as follows: 5 g pine needles feedstock was impregnated into a 90 mL solution mixture containing 16.22 g $FeCl_3 \cdot 6H_2O$ (0.67 mol/L) and 5.94 g $MnCl_2 \cdot 4H_2O$ (0.335 mol/L), the above mixed solution was stirred in a magnetic stirring water bath for 2 h at 80 °C. The obtained precursor was then dried at 105 °C for 24 h. After that, the dried sample was pyrolyzed with an OTF-1200X-L tubular furnace at 500 °C for 2 h with heating rate of 10 °C/min under a constant N_2 flow rate. The resulting bio-char products were crushed, washed and oven dried at 60 °C for 12 h before characterization. For comparison, the Fe–Mn binary oxides, Fe/bio-char and Mn/bio-char was synthesized by the same method without adding pine needles feedstock, $MnCl_2.4H_2O$ and $FeCl_3 \cdot 6H_2O$. Virgin bio-char was made by pyrolyzing pine needles feedstock directly following the calcining procedure above.

2.3. Characterization of catalysts

The Brunauer-Emmett-Teller (BET) specific surface areas of typical products were performed at 77 K in an AUTOSORB-1-MP system (Micromeritics Instrument Corporation, TRI-STAR3020, USA). In order to determine the crystal phases of catalysts, X-ray diffractometer (XRD) measurements were performed with a D/max-2500 X-ray diffractometer (Rigaku, Japan). Morphology of samples were examined by scanning electron microscope (SEM, Sirion 200). The element composition of catalyst was determined through an energy dispersive spectrometer (EDS, INCA X-Act). X-ray photoelectron spectrometry (XPS) was adopted to investigate the chemical states of elements by using an Axis Ultra spectrometer (Kratos, Japan) with Al Kα source ($h\nu = 1486.6$ eV). The magnetic properties of the materials were studied with vibrating sample magnetometer (VSM, SQUID-VSM (MPMS-3)). Fourier transform infrared (FT-IR) spectrophotometer (Spectrum BX; PerkinElmer Ltd., USA) was employed to characterize the surface functional groups.

2.4. Experimental procedure

Initially, 100 mL of naphthalene solution without catalyst and H_2O_2 was exposed to visible light to study the volatilization of

naphthalene under irradiation. The concentration of naphthalene was set as 30 mg/L according the concentration of naphthalene used in other researches and the typical concentration of naphthalene in wastewaters (Table S1). Typically, 100 mg of catalysts was added into 100 mL naphthalene solution (30 mg/L), and dark reaction (60 min) was performed to obtain adsorption/desorption equilibrium of naphthalene. Then, required amount of H_2O_2 was added to initiate the reaction under visible light irradiation. The visible light irradiation was supplied by a 300 W Xenon lamp with a 420 nm cutoff filter and the irradiation intensity is determined as 2.7 kW/m^2, which was 2.7 times as large as the irradiation intensity of the natural sunlight expected at the surface of the earth (1 kW/m^2). Samples were taken out regularly and then analyzed immediately after filtration through 0.45 μm Millipore membrane filters. To examine the adsorption of naphthalene by catalysts, control experiments were conducted with no addition of H_2O_2 and visible light irradiation, the results were presented in Fig. S1. To investigate the contribution of homogeneous Fenton reaction under acidic conditions, Fe^{2+} and Mn^{2+} were used as homogeneous catalysts to activate H_2O_2 for the removal of naphthalene and the results were shown in Fig. S5. The dosage of Fe^{2+} and Mn^{2+} used was the leaching amount under acidic conditions. To study the practical application value of FeMn/bio-char, the procedure of naphthalene degradation was also carried out under natural sunlight irradiation and the result was shown in Fig. S7. In the preliminary experiment on the real wastewater treatment, river water (Xiangjiang River, Changsha, China), tap water (derived from Changsha running-water company), industrial wastewater (obtained from Hebei Cangzhou Dahua CO.,LTD, China) and medical wastewater (obtained from Changsha 4th hospital, Changsha, China) were used as the solution for the preparation of 30 mg/L naphthalene wastewater. All experiments were performed in triplicate.

The detailed procedures for the treatment of bio-char by ethanol were provided in Supporting Information (Text 1).

2.5. Analytic methods

The concentrations of naphthalene were quantified by a high performance liquid chromatography (HPLC, Agilent 1260, USA) equipped with an Agilent TC-C18 column (150 mm × 4.6 mm, 5 μm) and an UV–vis photodiode array detector. The mobile phase was a mixture of distilled water and methanol (20: 80 (v/v)) at the detection wavelength of 240 nm. The column temperature was 25 °C and the flow rate was 1 mL/min.

The concentration of Fe and Mn released in solution after reaction were measured by flameless atomic absorption spectroscopy (AAS, PEAA700, Perkin Elmer, USA). The variation of H_2O_2 concentration during reaction was measured using a UV–vis spectrophotometer after complexation with metavanadate (Nogueira et al., 2005). The electron spin resonance (ESR) signals of spin-trapped radicals were conducted on a Bruker model ESR JESFA200 spectrometer using spin-trap reagent DMPO in water and methanol, respectively. The procedures for the determination of PFRs were presented in Supporting Information (Text 2).

The degradation intermediate products of naphthalene were analyzed using a QP2010-PLUS GC-MS system (SHIMADZU, Japan) equipped with a HP-5MS capillary column. The procedures for the determination of intermediate products were presented in Supporting Information (Text 3).

3. Results and discussion

3.1. Catalyst characterization

The surface properties of virgin bio-char and FeMn/bio-char was investigated using nitrogen adsorption and the results (Table S2) revealed that both as-prepared samples displayed mesoporous structures. It could be found from Table S2 that the BET surface and pore volume of bio-char increased after impregnation of Fe–Mn binary oxides, which increased from 14.14 m^2/g and 0.0219 cm^3/g to 159.05 m^2/g and 0.1111 cm^3/g, respectively. This might ascribe to the formation of new pores during impregnation and calcination. In general, catalyst with larger BET surface area possessed more active sites, which was conductive to the catalytic reaction.

The morphology of bio-char, Fe–Mn binary oxides and FeMn/bio-char were observed by SEM. As shown from Fig. 1, the virgin bio-char showed smooth surface and sharp edges (Fig. 1a), while Fe–Mn binary oxides obviously aggregated into a sphere (Fig. 1b). As for FeMn/bio-char, Fe–Mn binary oxides were homogeneously diffused onto the surface of bio-char without obvious gathering (Fig. 1c). EDS analysis shown in Fig. 1d indicated the coexistence of Fe, Mn, C and O.

The XRD patterns of virgin bio-char, Fe/bio-char, Mn/bio-char and FeMn/bio-char were presented in Fig. 2a. As for bio-char, the XRD peak at $2\theta = 20–25°$ was regarded as the graphite amorphous structure of bio-char (Ouyang et al., 2017). The peak intensity of carbon became weaker with the doping of Fe–Mn binary oxides, suggesting that the introduction of Fe–Mn binary oxides might cover the surface of bio-char. For Fe/bio-char, the diffraction peaks at $2\theta = 18.3°$, 30.1°, 35.5°, 36.9°, 43.1°, 53.5°, 56.9° and 62.6° were ascribed to Fe_3O_4 (JCPSD 18–0803), and the diffraction peaks at $2\theta = 33°$, 49° and 54° were attributed to Fe_2O_3 (JCPDS 33–0664). Diffraction lines for Mn_3O_4 ($2\theta = 18°$, 28.9°, 31°, 32.4°, 36.04°, 44.4°, 50.7°, 58.6°, 60.0°, 64.6°) were detected over Mn/bio-char. In addition, the peak appeared around $2\theta = 37.9°$ was attributed to Mn_2O_3 (Zhao et al., 2018a). While the peaks of manganese oxides were not detected on the surface of FeMn/bio-char. This might attribute to the fact that the amount of Mn oxides was too low to form crystalline phase on the basis of monolayer dispersion theory (Xie and Tang, 1990). Besides, the XRD patterns of FeMn/bio-char show stronger and narrower peaks demonstrating high crystallinity of the resulted samples.

Fig. 2b showed the FTIR spectra of bio-char, FeMn/bio-char before and after reaction. In Fig. 2b, five stretching vibration bands could be observed for bio-char at wavelengths at 3440, 1580, 1388,

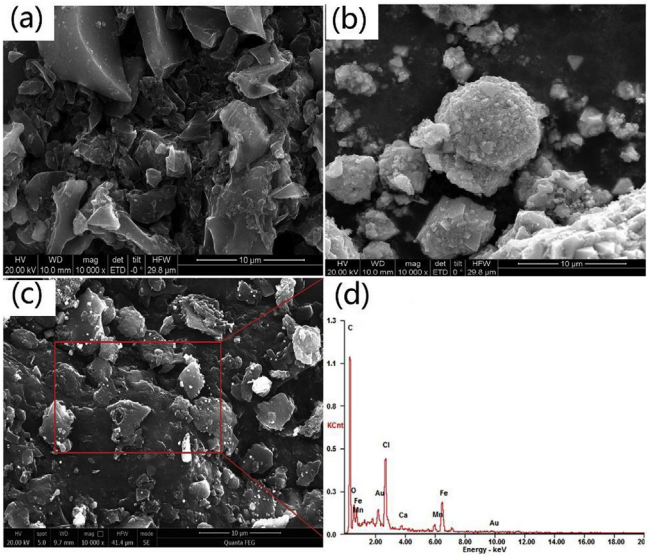

Fig. 1. SEM images of (a) bio-char, (b) Fe–Mn binary oxides, (c) FeMn/bio-char and (d) EDX of FeMn/bio-char.

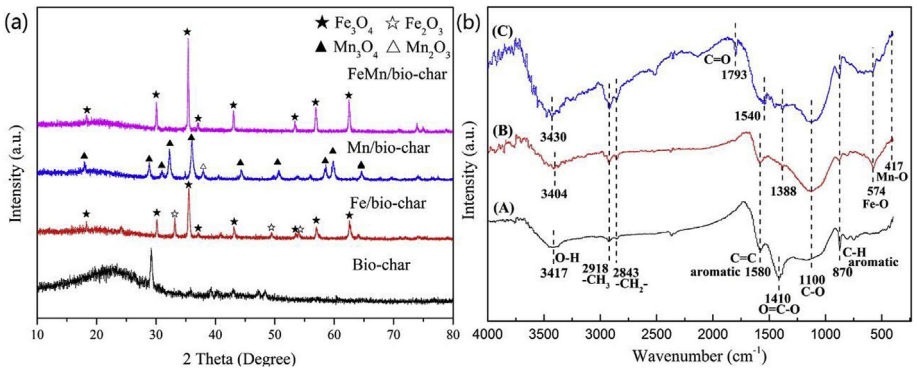

Fig. 2. (a) XRD patterns of virgin bio-char, Fe/bio-char, Mn/bio-char and FeMn/bio-char; (b) FT-IR spectra of (A) bio-char, (B) FeMn/bio-char before reaction and (C) FeMn/bio-char after reaction.

1100 and 870 cm^{-1}, respectively, being assigned to −OH, C=C, carboxyl O=C−O, alkoxy C−O and aromatic C−H groups (Tang et al., 2016). Meanwhile, the intense adsorption band at 2918 cm^{-1} and 2843 cm^{-1} verified asymmetric and symmetric stretching of CH_2 groups. For FeMn/bio-char composite, the peaks centered at 574 cm^{-1} and 417 cm^{-1} can be assigned to the Fe−O and Mn−O bending vibrations (Wan and Wang, 2017b). Compared with FTIR patterns of bio-char and FeMn/bio-char samples, we could conclude that impregnation leads to slight shift in stretching band of surface functional groups such as −OH (from 3417 to 3404 cm^{-1}) and −COOH (from 1410 to 1388 cm^{-1}), suggesting that Fe−Mn binary oxides were bounded on the surface of bio-char via interactions with these functional groups (Yang et al., 2018a). In the case of FeMn/bio-char after reaction, a new peak emerged at 1793 cm^{-1}, which may be due to the presence of carbonyl units, such as lactone groups (Li et al., 2017a).

Fig. 3a presented the survey spectra of FeMn/bio-char before and after reaction. The elements of C (284.8 eV), O (531.1 eV), Fe 287 (711.0 eV, 724.7 eV) and Mn (641.4 eV, 653.6 eV) could be observed from the survey spectra of both catalysts. Fig. 3b showed the C 1S peak of FeMn/bio-char before and after reaction. From the spectrum before reaction, we can see that binding energy at 284.6 eV, 285.1 eV, 286.1 eV and 288.9 eV corresponded to C=C, C−C, C−O and O−C=O respectively (Ouyang et al., 2017). The appearance of C=O after reaction could be ascribed to the byproduct of ring-opening reaction of naphthalene, which was consistent with FTIR analysis. From the XPS spectrum of Fe 2p (Fig. 3c), two main asymmetric peaks located at 711.0 eV and 724.7 eV could be ascribed to Fe $2p_{3/2}$ and Fe $2p_{1/2}$, respectively (Wan and Wang, 2017b). For Fe $2p_{3/2}$, the peak at 710.5 eV was attributed to Fe (II), another two binding energies at 711.8 eV and 713.2 eV were related to Fe (III) in different forms. Besides, the shake-up satellite peak at about 718.6 eV suggested the presence of Fe (III) (Du et al., 2018). For high-resolution XPS spectra of Mn 2p (Fig. 3d), two main peaks assigned to Mn $2p_{3/2}$ and Mn $2p_{1/2}$ were observed at 641.4 eV and 653.6 eV, respectively. The Mn $2p_{3/2}$ peak can be divided into two peaks: Mn (II) (641.2 eV) and Mn (III) (642.8 eV) (Du et al., 2018). Furthermore, a satellite peak at 646.9 eV may be ascribed to the presence of Mn (II) (Zhou et al., 2016). However, some values shifted after the reaction with H_2O_2 and naphthelene. From the deconvolution of Mn 2p and Fe 2p envelops before reaction, the peak area ratio of Mn (III)/Mn (II) was about 0.61 and the percentage of Fe (II) and Fe (III) were 49% and 51% respectively. While according to the deconvolution of Fe 2p and Mn 2p envelops after reaction, the Mn (III)/Mn (II) value decreased to 0.37 and the percentage of Fe (II) and Fe (III) changed to 43.7% and 56.3% respectively. These changes displayed that a good portion of Fe (II) and Mn (III) of used FeMn/bio-char was transformed to Fe (III) and Mn (II), indicating that both Mn (II)/Mn (III) and Fe (II)/Fe (III) species were involved in activation of H_2O_2 by FeMn/bio-char.

ESR was used to verify the existence of PFRs in bio-char and FeMn/bio-char samples and the result was shown in Fig. 4. The result suggested that for both bio-char and FeMn/bio-char, the pronounced ESR signals were observed. Moreover, the ESR intensity of FeMn/bio-char was higher than that of bio-char, suggesting that the metal treatment would increase the concentration of PFRs in composite. The similar effect was found by Fang et al. (2015).

The room temperature magnetization curves and the magnetization property data of bare Fe−Mn binary oxides and FeMn/bio-char composite were shown in Fig. S2 and Table 1. The saturated magnetization (Ms) of FeMn/bio-char composite was lower than the Ms of bare Fe−Mn binary oxides, which might be attributed to the existence of bio-char. With large saturated magnetization, FeMn/bio-char could be manipulated through external magnetic field, such as magnet (Fig. S2, inset). Moreover, owing to the low remnant magnetization (Mr) values, FeMn/bio-char composite could easily re-disperse in a solution for reuse after separating (Nguyen et al., 2011).

3.2. Degradation of naphthalene

3.2.1. Naphthalene removal using different catalysts

The removal of naphthalene by bio-char, Fe−Mn binary oxides and FeMn/bio-char were presented in Fig. 5a and the decomposition behavior of H_2O_2 by different catalysts were shown in Fig. 5b. Under dark condition, the adsorption equilibrium between naphthalene and catalysts were obtained within 60 min (Fig. S1), approximately 23.4%, 20.1% and 48.9% of naphthalene was removed by bio-char, Fe−Mn binary oxides and FeMn/bio-char, respectively. The optimal adsorption performance of FeMn/bio-char suggested that there is a synergistic promoting effect between Fe−Mn binary oxides and bio-char. After addition of H_2O_2 and visible light irradiation, the degradation efficiency of naphthalene significantly improved. As seen from Fig. 5a, naphthalene was decreased by 8.5% without catalysts and H_2O_2 due to volatilization. The degradation of naphthalene is ordered as FeMn/bio-char > FeMn/binary oxides > bio-char > H_2O_2 alone, and the specific value after 148 min is 75.8%, 46.9%, 44.9% and 11.5%, respectively. The removal efficiency with H_2O_2 alone indicated that H_2O_2 could hardly degrade naphthalene under visible light irradiation. The lower degradation efficiency of Fe−Mn binary oxides might be attributed to the catalyst aggregation, which weakened the accessibility of reactants towards the active sites. As shown in Fig. 1, the addition of bio-char

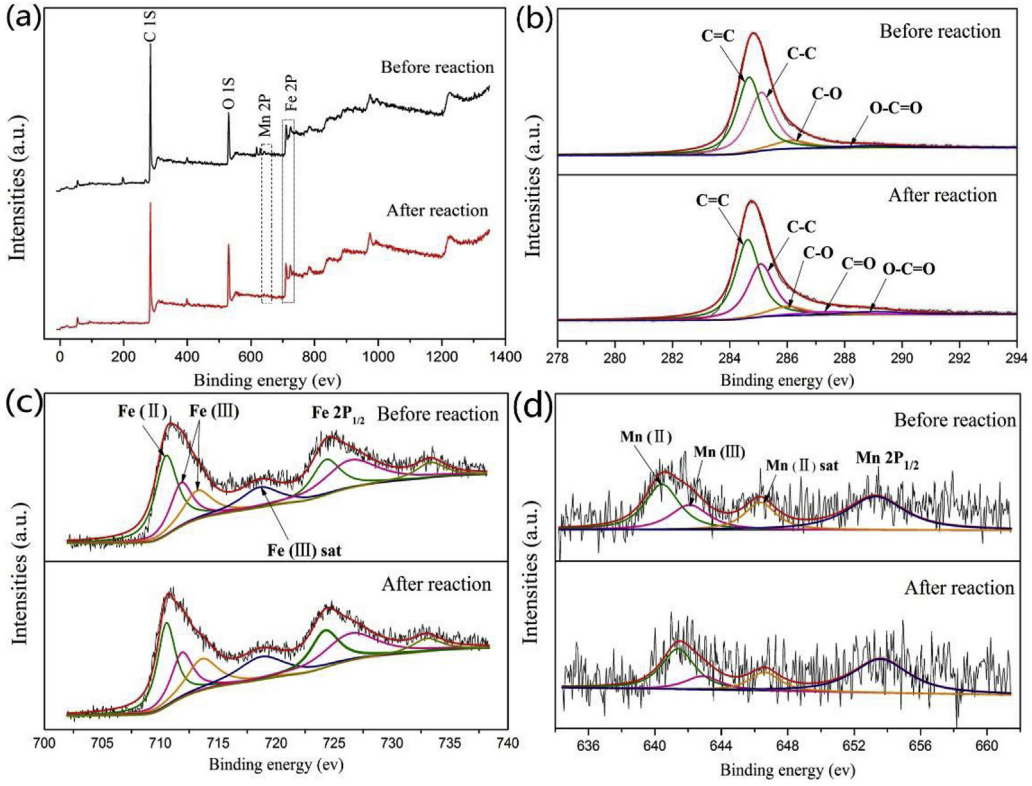

Fig. 3. XPS spectra of FeMn/bio-char before and after reaction: (a) survey, (b) C 1s, (c) Fe 2p and (d) Mn 2p.

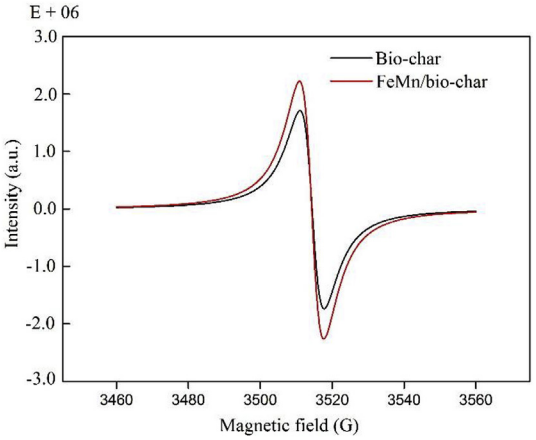

Fig. 4. ESR spectra of bio-char and FeMn/bio-char samples.

Table 1
The magnetic properties of Fe–Mn binary oxides and FeMn/bio-char.

Sample	Hc (Oe)	Mr (emu g^{-1})	Ms (emu g^{-1})
Fe–Mn binary oxides	143	9.95	84.45
FeMn/bio-char	44.43	1.82	32.664

obviously alleviated the agglomeration of material, which was mainly responsible for the higher catalytic performance of FeMn/bio-char compared to Fe–Mn binary oxides. In addition, FeMn/bio-char showed a higher catalytic capability towards activating H_2O_2 for naphthalene removal than bio-char, probably due to the increasing concentration of PFRs and the activation of H_2O_2 by Fe–Mn binary oxides (Eqs. (1) and (2)). As stated above, the synergistic effects of bio-char and Fe–Mn binary oxides were significant to the enhancement of catalytic activity.

For comparison, Fe/bio-char and Mn/bio-char were also taken into consideration. The pseudo-first-order plots of H_2O_2 decomposition under different catalysts were also analyzed (Fig. S3). As shown in Fig. 5 and Fig. S3, Mn/bio-char composite exhibited the fastest H_2O_2 decomposition, nearly 89.3% of H_2O_2 was decomposed within 88 min ($k = 0.029$ min^{-1}), whereas only 63.7% naphthalene was degraded by Mn/bio-char composite under visible light irradiation. This might be ascribed to the scavenging of •OH and less generation of $•O_2^-$ in Mn/bio-char/H_2O_2 system. As shown from Fig. S4, no apparent difference of peak intensities of DMPO-•OH could be observed between FeMn/bio-char and Mn/bio-char, though Mn/bio-char exhibited faster decomposition rate of H_2O_2 than FeMn/bio-char. This result suggested that the amount of effective •OH generated in Mn/bio-char/H_2O_2 system was not larger than that in FeMn/bio-char/H_2O_2 system, which was possibly because the •OH generated rapidly in a short time would be quenched (Zhong et al., 2014; Xue et al., 2018). Additionally, we can see from Fig. S4 that the peak intensities of DMPO-$•O_2^-$ in Mn/bio-char/H_2O_2 system was much weaker than that in FeMn/bio-char/H_2O_2 system, indicating less generation of $•O_2^-$ in Mn/bio-char/H_2O_2 system. In comparison, the decomposition of H_2O_2 with Fe/bio-char as catalyst was relatively slower ($k = 0.006$ min^{-1}), about 39.2% of H_2O_2 was decomposed in the presence of Fe/bio-char. The faster degradation rate of H_2O_2 by Mn/bio-char compared to Fe/bio-char might be ascribed to the reaction between Mn (III) and H_2O_2, since the order of reactivity between transition ions and H_2O_2 is Mn (III)>Co (III)> Fe (III) (Wan and Wang, 2017a). Meanwhile, 63% of naphthalene was degraded by Fe/bio-char. Both degradation values of naphthalene by Mn/bio-char and Fe/bio-char were not comparable with that of FeMn/bio-char, that is to say, the catalysts combining iron and manganese are more efficient in photo-Fenton

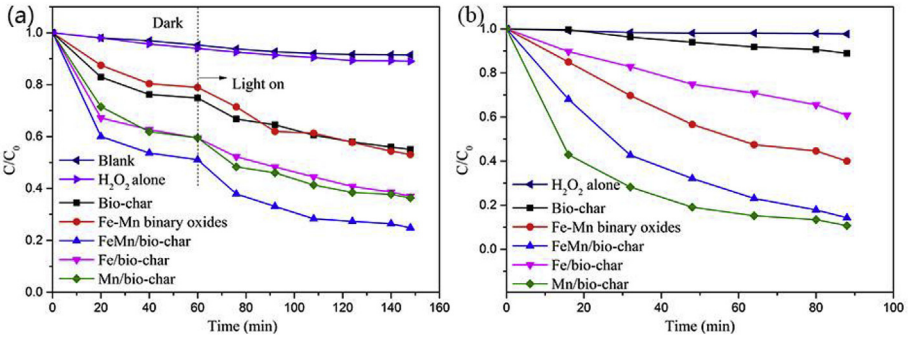

Fig. 5. (a) Degradation of naphthalene and (b) decomposition of H_2O_2 by the as-prepared samples. Experiments conditions: naphthalene concentration = 30 mg/L; H_2O_2 concentration = 100 mM; catalyst loading = 1.0 g/L; initial pH = 5.6.

reaction. Therefore, FeMn/bio-char was selected for further study.

$$\equiv Fe\ (II) + H_2O_2 \rightarrow \equiv Fe\ (III) + \bullet OH + OH^- \quad (1)$$

$$\equiv Mn\ (II) + H_2O_2 \rightarrow \equiv Mn\ (III) + \bullet OH + OH^- \quad (2)$$

3.2.2. Effects of catalyst dosage on naphthalene degradation

To select optimum FeMn/bio-char dosage, the naphthalene degradation by FeMn/bio-char was investigated under different initial dosage. As shown in Fig. 6a, FeMn/bio-char (0.25 g/L, 0.5 g/L, 1 g/L) and H_2O_2 within the 148 min reaction time removed 66.7%, 70.1% and 77.1% of the naphthalene. As the amount of FeMn/bio-char dosage increased, there would be more active sites on catalyst surface. In addition, more catalyst might increase the adsorption of naphthalene. But there was no significant increase of degradation efficiency when further increasing the dosage to 1.5 g/L and 2.0 g/L. On the one hand, excessive catalyst in the solution might lead to the loss of available radiation because of light scattering (Zhong et al., 2012). And consequently, the regeneration of Fe (II) would be decreased due to the less effective utilization of visible light (see detail discussion in section *3.2.5*). On the other hand, the scavenging of •OH would occur when presenting excessive catalyst (Eq. (3)). Hence, 1 g/L was the optimal dosage for the sample.

$$\equiv M\ (II) + \bullet OH \rightarrow \equiv M\ (III) + OH^- \text{ (M: Fe or Mn)} \quad (3)$$

3.2.3. Effects of H_2O_2 concentration on naphthalene degradation

The effect of H_2O_2 dosage (25 mM–200 mM) on naphthalene degradation was shown in Fig. 6b. From Fig. 6b, the degradation efficiency was 64.6%, 71.2%, 75.2% and 82.2% corresponding to the concentration of H_2O_2 at 25, 50, 100 and 150 mM. With the addition of H_2O_2, there would be more •OH generated to degrade high concentration of naphthalene, which leads to the increase of naphthalene removal efficiency. However, when H_2O_2 concentration increased from 150 mM to 200 mM, the degradation of naphthalene decreased from 82.1% to 74.9%, which can be attributed to the scavenging of •OH by excess H_2O_2 (Eq. (4)). Besides, excess H_2O_2 can also compete with naphthalene for the adsorption sites on catalyst surface (Wan and Wang, 2017b). Thus, 150 mM H_2O_2 was an optimal concentration and utilized in subsequent experiments.

$$H_2O_2 + \bullet OH \rightarrow H_2O + HO_2\bullet \quad (4)$$

3.2.4. Effects of pH on naphthalene degradation

The degradation efficiency of naphthalene under different initial pH was also explored. As seen from Fig. 6c, naphthalene was degraded 77.3%, 82.8%, 80.1% and 79.7% under the initial pH of 3.0, 5.0, 7.0 and 9.0, respectively. This result suggested that the FeMn/bio-char can work effectively under a wide range of pH. While a pH 3 solution resulted in a minimal efficiency according to our experiments, which was different from the previous studies (Hu et al., 2011). We further studied the removal of naphthalene by homogeneous photo-Fenton reaction under acidic conditions and the results were presented in Fig. S5. Since the leaching amount of Fe and Mn after reaction was 1.03 mg/L and 2.29 mg/L, respectively under acidic conditions. This may not the optimum catalyst dosage in homogeneous photo-Fenton reaction when H_2O_2 concentration was 150 mM. Hence the degradation kinetic is still governed by heterogeneous Fenton reaction in FeMn/bio-char/H_2O_2 system under acidic conditions from the results in Fig. S5. To further explain the relatively lower degradation efficiency of naphthalene under acidic conditions. We studied the change of solution pH during reaction under different initial pH. As shown from Fig. S6, when the initial pH was 3, 5, 5.6, 7 and 9 respectively, the solution pH dropped rapidly to 2.45, 3.0, 3.02, 3.3 and 7.06 respectively after photo-Fenton reaction and then changed slightly in the following degradation process. The decrease of solution pH might be ascribed to the generation of acidic intermediates during naphthalene degradation. Hence, when the initial pH was 3, the solution pH would rapidly decrease to 2.45 after reaction, the formation of $Fe(H_2O)_6^{3+}$ at lower acid environment would restrain the reaction between H_2O_2 and catalyst, leading to the less generation of •OH (Gao et al., 2018), which might be reasonable for the lower efficiency at initial pH of 3. Additionally, previous studies which obtained lower degradation efficiency at acidic conditions have been presented in Table S3. When the initial pH was set as 9.0, a slower degradation rate of naphthalene was observed, because the generation of •OH from H_2O_2 was gradually restricted and the oxidation potential of •OH also decreased with the pH increasing. While a relatively higher efficiency was obtained at pH 9, which would be ascribed to the better adsorption of naphthalene in higher pH (Cheng et al., 2018b). This was probably because the solutions at higher pH had different ionic strength, further affecting adsorption capacity (Lair et al., 2008). Moreover, FeMn/bio-char had relatively high degradation efficacy at neutral initial pH, so there was no need to control the pH of wastewater.

3.2.5. Effects of visible light irradiation on naphthalene degradation

To explore the role of light in catalytic oxidation, experiment was further conducted under dark condition with FeMn/bio-char as catalyst. As shown in Fig. 6d, the degradation ratio of naphthalene

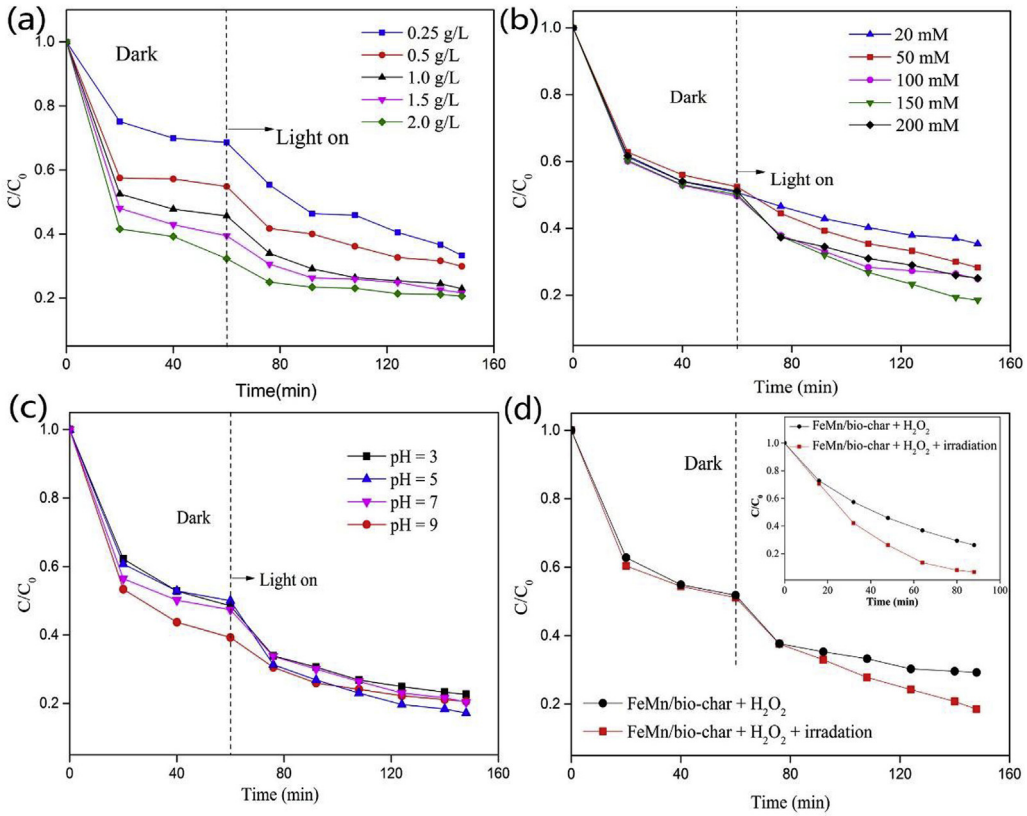

Fig. 6. Effects of (a) catalyst dosage, (b) H_2O_2 concentration, (c) pH and (d) visible light irradiation (the inset shows the effect of visible light irradiation in decomposition of H_2O_2) in degradation rates of naphthalene. Experimental conditions: (a) naphthalene concentration = 30 mg/L; H_2O_2 concentration = 100 mM; initial pH = 5.6; (b) naphthalene concentration = 30 mg/L; catalyst loading = 1.0 g/L; initial pH = 5.6; (c) naphthalene concentration = 30 mg/L; H_2O_2 concentration = 150 mM; catalyst loading = 1.0 g/L; (d) naphthalene concentration = 30 mg/L; H_2O_2 concentration = 150 mM; catalyst loading = 1.0 g/L; initial pH = 5.6.

declined to 69.8% for FeMn/bio-char composite in the dark. Moreover, the decomposition efficiency of H_2O_2 was greatly declined with the absence of visible light irradiation (Fig. 6d, inset). The remarkable decrease of catalytic efficiency under dark condition possibly because photo-reduction of Fe (III) also played an important role in naphthalene degradation reaction (Li et al., 2017b), since the regeneration of Fe (II) could be accelerated via photo-reduction of Fe (III) (Eq. (5)) (Cai et al., 2016; Li et al., 2017b; Diao et al., 2018; Ruales-Lonfat et al., 2015). Simultaneously, the forming Fenton's reagent Fe (II)/H_2O_2 may further oxidize the contaminants by Fenton reaction (Eq. (1)). Furthermore, we studied the degrading activity of FeMn/bio-char towards naphthalene under natural sunlight irradiation to investigate the practical application value of this catalyst (Location: Hunan University, N28°10′54″ E112°56′18″; Date: May 9, 2019; Weather: Cloudy day). As seen from Fig. S7, 83.7% of naphthalene was degraded within 148 min under sunlight irradiation, indicating that FeMn/bio-char could effectively remove naphthalene under natural sunlight irradiation. The obtained results suggested that this photo-Fenton catalyst exhibited good potentials in environmental remediation process.

$$\equiv Fe\ (III) + OH^- + h\upsilon \rightarrow \equiv Fe\ (II) + \bullet OH \quad (5)$$

3.3. Identification of reactive radical species

The free radical trapping experiments were conducted to identify the reactive oxygen radicals in FeMn/bio-char/H_2O_2 photo-Fenton system. Benzoquinone (BQ) and tert-butyl alcohol (TBA) were used as scavengers of superoxide radicals ($\bullet O_2^-$) and •OH, respectively (Gao et al., 2018; Yang et al., 2018b). As seen from Fig. 7a, the addition of TBA rapidly decreased the degradation efficiency of naphthalene, while the efficiency was scarcely decreased with the addition of BQ. The results indicated that •OH was the main active species, but $\bullet O_2^-$ played minor roles in the photo-Fenton process.

To further verify the free radicals species, ESR with DMPO in aqueous solution was carried out to further determine the free radicals species in this FeMn/bio-char/H_2O_2 photo-Fenton system. The results were shown in Fig. 7b. The intensity of ESR signal depends on concentration of radical's concentration. Obviously, the peak intensities of DMPO-•OH radical increased with time going on. In addition, the signals of DMPO-$\bullet O_2^-$ were also detected under visible light irradiation, indicating that both •OH and $\bullet O_2^-$ were generated during reaction. However, the intensity signals of DMPO-$\bullet O_2^-$ were much weaker than DMPO- •OH. This result suggested that •OH was the primary oxidative species in this heterogeneous photo-Fenton system and $\bullet O_2^-$ partially contributed the degradation of naphthalene, which were consistent with the results of free radical trapping experiments.

3.4. Reaction mechanism

The mechanism of FeMn/bio-char/H_2O_2 photo-Fenton system in the removal of naphthalene was summarized in Fig. 8. On the one hand, PFRs on the surface of samples could directly activate H_2O_2 to generate •OH and further degraded naphthalene. To further testify the catalytic performance of PFRs during photo-Fenton reaction, ethanol was used as the scavenger to decrease the concentration of

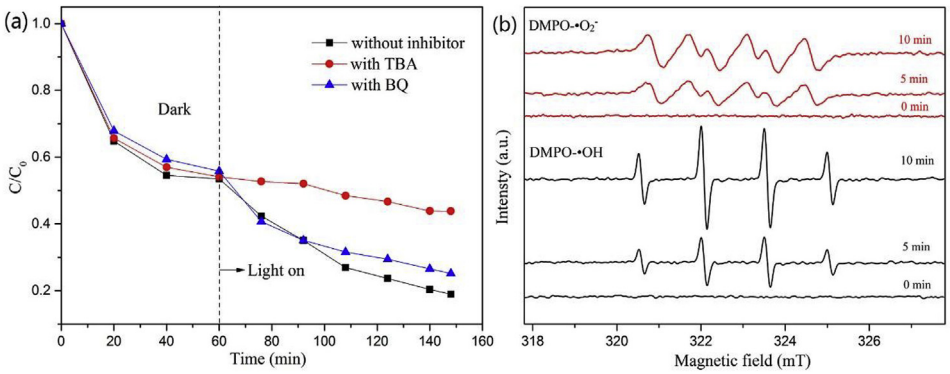

Fig. 7. (a) Degradation of naphthalene with different inhibitor. Experimental conditions: naphthalene concentration = 30 mg/L; H_2O_2 concentration = 150 mM; catalyst loading = 1.0 g/L; initial pH = 5.6. (b) DMPO spin-trapping ESR spectra of FeMn/bio-char aqueous dispersion (for DMPO-•OH) and methanol dispersion (for DMPO-$•O_2^-$) under irradiation of xenon lamp.

PFRs in bio-char (Zhao et al., 2018b). As seen from Fig. S8, the removal efficiency of naphthalene decreased with the increase of the concentration of scavenger. The obtained result further confirmed the decent effect of PFRs in this photo-Fenton process. On the other hand, the redox catalytic cycle of Fe (II)/Fe (III) and Mn (II)/Mn (III) in FeMn/bio-char/H_2O_2 photo-Fenton system (Eqs. (1) and (2)) can produce •OH to oxide naphthalene. In this cyclical reaction, Mn (III) can be reduced by Fe (II) thermodynamically according to the redox potential of E^0 (Mn (III)/Mn (II)) = 1.51 V and E^0 (Fe (III)/Fe (II)) = 0.771V (Eq. (6)), which promotes the electron transfer in the reaction system and breaks the restriction that the conversion of Mn (III) to Mn (II) was dependent on H_2O_2 (Eq. (7)). Simultaneously, Fe (II) could be regenerated via photolysis of Fe (III) (Eq. (5)). The efficient regeneration of Fe (II) and Mn (II) could contribute to the remarkable increase of naphthalene degradation activity.

$$\equiv Fe\ (II) + \equiv Mn\ (III) \rightarrow \equiv Mn\ (II) + \equiv Fe\ (III) \quad (6)$$

$$\equiv Mn\ (III) + H_2O_2 \rightarrow \equiv Mn\ (II) + HO_2\bullet + H^+ \quad (7)$$

3.5. Identification of intermediates and transformation pathway

The main intermediates identification and confirmation by GC-MS analysis are presented in Table S6 and the possible degradation pathways were proposed based on above intermediates. The •OH formed from FeMn/bio-char photo-Fenton system could attack α-position of naphthalene (1) and led to the structure (2) (Fig. 9). An abstraction of H from structure (2) yielded the formation of 1-naphthol (3) which was the primary intermediates of naphthalene degradation (Andas et al., 2014). The second possibility was the formation of 2-formylcinnamaldehyde (5) by an attack of $•O_2^-$ on the naphthalene which produced an unstable endoperoxide (4) (Lair et al., 2008). While the direct attack by $•O_2^-$ was rare since $•O_2^-$ was not the primary active radicals in this study. In addition, •OH attacking structure (5) resulted in the formation of 1, 2-Benzenedicarboxaldehyde (6) and finally led to the generation of 1, 2-benzenedicarboxylic acid (7) (Yang et al., 2018b). Then structure (7) further reacted with •OH to form 1-Propene-1, 2, 3-tricarboxylic acid (8) (Garcia-Segura et al., 2013).

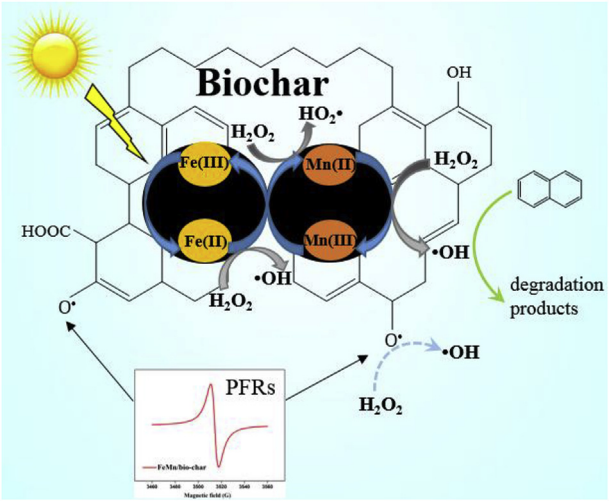

Fig. 8. Proposed mechanism of FeMn/bio-char activating H_2O_2 for naphthalene degradation.

3.6. Reuse of catalyst and application on the real wastewater treatment

The stability of FeMn/bio-char is significantly important in actual application. Hence four consecutive experiments were conducted to investigate the stability of FeMn/bio-char. As seen from Fig. 10a, the removal efficiency after four cycles was 82.2%, 75.3%, 72.2% and 71.0%, respectively. The loss of activity might be ascribed to the following reasons. Firstly, the concentration of PFRs would decrease after addition of H_2O_2 (Fang et al., 2014) and the slight leaching of metal ions on the catalyst would lead to the loss of active sites. Secondly, some residual by-products might block the active catalytic sites and further hindered the degradation efficiency of organics (Nguyen et al., 2011). Besides, the XRD pattern of FeMn/bio-char before and after use was presented in Fig. 10b to examine the crystal structure of catalyst. No apparent changes can be seen from Fig. 10b, further confirming the stability of the catalyst. Additionally, the leaching amount of Fe and Mn after reaction was 0.55 mg/L and 2.03 mg/L, respectively.

Water matrix is an important factor in actual applications. Hence the difference between actual wastewater and simulated wastewater could significantly impact the degradation efficiency of target contaminant (naphthalene). In this study, the removal efficiency of naphthalene in ultrapure water, tap water (Changsha Running-water Company), river water (taken from Xiangjiang River, Changsha), industrial wastewater (obtained from Hebei Cangzhou Dahua CO., LTD, China) and medical wastewater (obtained from Changsha 4th hospital, Changsha, China) were investigated (Fig. S9). The results (Fig. S9) showed that the removal efficiency of naphthalene in ultrapure water, tap water, river water,

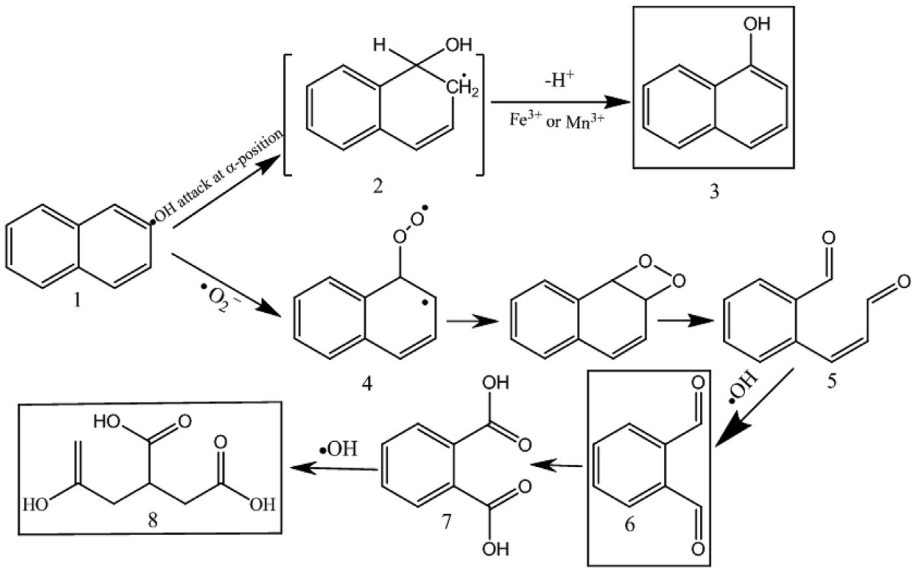

Fig. 9. Possible pathways of naphthalene degradation.

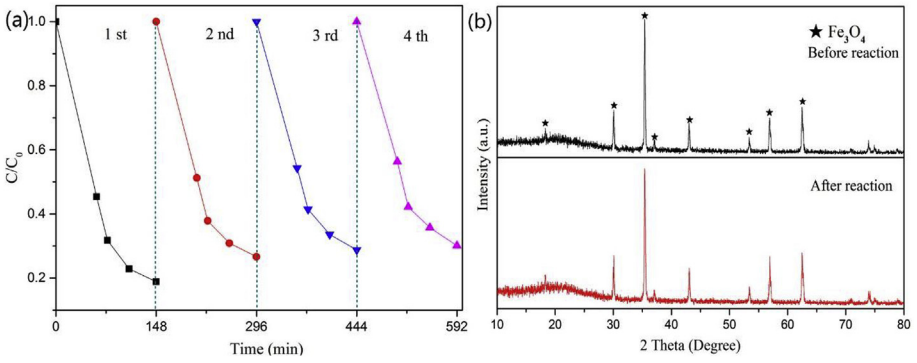

Fig. 10. (a) The catalytic activity of reused FeMn/bio-char on naphthalene degradation. Experimental conditions: naphthalene concentration = 30 mg/L; H_2O_2 concentration = 150 mM; catalyst loading = 1.0 g/L; initial pH = 5.6. (b) XRD patterns of FeMn/bio-char before and after reaction.

industrial wastewater and medical wastewater was 82.2%, 80.4%, 79.5%, 70.7% and 72.3% respectively. The consumption of •OH by the organic matters in industrial wastewater and medical wastewater might be responsible for the relatively lower removal of naphthalene in these two wastewaters. The obtained results showed the proposed photo-Fenton process could remove most of the naphthalene in different types of polluted waters, suggesting that this photo-Fenton catalyst exhibited good potentials for treatment of actual wastewater.

4. Conclusion

- In this study, the bio-char based catalysts were successfully synthesized via wet impregnation method with one-step pyrolysis. Moreover, the FeMn/bio-char exhibited pronounced photo-Fenton reactivity than Fe/bio-char and Mn/bio-char owing to the synergistic effects of iron and manganese.
- The FeMn/bio-char/H_2O_2 photo-Fenton system can work effectively at a wide pH range. Additionally, FeMn/bio-char showed good stability and reusability during photo-Fenton process.
- Bio-char and Fe–Mn binary oxides presented synergistic promoting effect in this photo-Fenton system. The combination of these two materials not only enhanced the adsorption capacity of contaminant but also accelerated the activation towards H_2O_2. The regeneration of Fe (II) and Mn (II) and the increase concentration of PFRs mainly responsible for the remarkable increase of removal efficiency.
- A further study conducted in river water, tap water, industrial wastewater and medical wastewater confirmed the application feasibility of FeMn/bio-char in actual wastewater treatment.
- This work may bring valuable insights for the potential environmental applications of modified bio-char.

Declaration of interest statement

There are no conflicts to declare.

Acknowledgments

This study was financially supported by the Program for the National Natural Science Foundation of China (51779090, 51408206, 51709101, 51579098, 51521006, 41601272), Science and Technology Plan Project of Hunan Province (2017SK2243, 2018SK20410, 2016RS3026), the National Program for Support of Top–Notch Young Professionals of China (2014), the Program for

New Century Excellent Talents in University (NCET-13-0186), the Program for Changjiang Scholars and Innovative Research Team in University (IRT-13R17), the Fundamental Research Funds for the Central Universities (531107050978, 531107051080, 531109200027), and Hunan Provincial Innovation Foundation for Postgraduate (CX2018B155).

Appendix A. Supplementary data

Supplementary data to this article can be found online at https://doi.org/10.1016/j.watres.2019.05.081.

References

Andas, J., Adam, F., Rahman, I.A., Taufiq-Yap, Y.H., 2014. Optimization and mechanistic study of the liquid-phase oxidation of naphthalene over biomass-derived iron catalyst. Chem. Eng. J. 252, 382–392.

An, Y.J., Carraway, E.R., 2002. PAH degradation by UV/H_2O_2 in perfluorinated surfactant solutions. Water Res. 36 (1), 309–314.

Babuponnusami, A., Muthukumar, K., 2014. A review on Fenton and improvements to the Fenton process for wastewater treatment. J. Environ. Chem. Eng. 2 (1), 557–572.

Cai, C., Zhang, Z., Liu, J., Shan, N., Zhang, H., Dionysiou, D.D., 2016. Visible light-assisted heterogeneous Fenton with $ZnFe_2O_4$ for the degradation of Orange II in water. Appl. Catal. B: Environ. 182, 456–468.

Cheng, M., Liu, Y., Huang, D., Lai, C., Zeng, G., Huang, J., Liu, Z., Zhang, C., Zhou, C., Qin, L., Xiong, W., Yi, H., Yang, Y., 2019. Prussian blue analogue derived magnetic Cu-Fe oxide as a recyclable photo-Fenton catalyst for the efficient removal of sulfamethazine at near neutral pH values. Chem. Eng. J. 362, 865–876.

Cheng, M., Zeng, G., Huang, D., Lai, C., Liu, Y., Zhang, C., Wang, R., Qin, L., Xue, W., Song, B., Ye, S., Yi, H., 2018b. High adsorption of methylene blue by salicylic acid-methanol modified steel converter slag and evaluation of its mechanism. J. Colloid Interface Sci. 515, 232–239.

Cheng, M., Zeng, G., Huang, D., Lai, C., Liu, Y., Zhang, C., Wan, J., Hu, L., Zhou, C., Xiong, W., 2018a. Efficient degradation of sulfamethazine in simulated and real wastewater at slightly basic pH values using Co-SAM-SCS/H_2O_2 Fenton-like system. Water Res. 138, 7–18.

Diao, Y., Yan, Z., Guo, M., Wang, X., 2018. Magnetic multi-metal co-doped magnesium ferrite nanoparticles: an efficient visible light-assisted heterogeneous Fenton-like catalyst synthesized from saprolite laterite ore. J. Hazard. Mater. 344, 829–838.

Du, X., Li, C., Zhao, L., Zhang, J., Gao, L., Sheng, J., Yi, Y., Chen, J., Zeng, G., 2018. Promotional removal of HCHO from simulated flue gas over Mn-Fe oxides modified activated coke. Appl. Catal. B: Environ. 232, 37–48.

Fang, G., Gao, J., Liu, C., Dionysiou, D.D., Wang, Y., Zhou, D., 2014. Key role of persistent free radicals in hydrogen peroxide activation by biochar: implications to organic contaminant degradation. Environ. Sci. Technol. 48 (3), 1902–1910.

Fang, G., Liu, C., Gao, J., Dionysiou, D.D., Zhou, D., 2015. Manipulation of persistent free radicals in biochar to activate persulfate for contaminant degradation. Environ. Sci. Technol. 49 (9), 5645–5653.

Gao, J., Liu, Y., Xia, X., Wang, L., Dong, W., 2018. $Fe_{1-x}Zn_xS$ ternary solid solution as an efficient Fenton-like catalyst for ultrafast degradation of phenol. J. Hazard. Mater. 353, 393–400.

Garcia-Segura, S., Bellotindos, L.M., Huang, Y.H., Brillas, E., Lu, M.C., 2016. Fluidized-bed Fenton process as alternative wastewater treatment technology—a review. J. Taiwan Inst. Chem. E. 67, 211–225.

Garcia-Segura, S., Salazar, R., Brillas, E., 2013. Mineralization of phthalic acid by solar photoelectro-Fenton with a stirred boron-doped diamond/air-diffusion tank reactor: influence of Fe^{3+} and Cu^{2+} catalysts and identification of oxidation products. Electrochim. Acta 113 (4), 609–619.

Hu, X., Liu, B., Deng, Y., Chen, H., Luo, S., Sun, C., Yang, P., Yang, S., 2011. Adsorption and heterogeneous Fenton degradation of 17α-methyltestosterone on nano Fe_3O_4/MWCNTs in aqueous solution. Appl. Catal. B: Environ. 107 (3–4), 274–283.

Lai, C., Huang, F., Zeng, G., Huang, D., Qin, L., Cheng, M., Zhang, C., Li, B., Yi, H., Liu, S., Li, L., Chen, L., 2019b. Fabrication of novel magnetic $MnFe_2O_4$/bio-char composite and heterogeneous photo-Fenton degradation of tetracycline in near neutral pH. Chemosphere 224, 910–921.

Lai, C., Wang, M., Zeng, G., Liu, Y., Huang, D., Zhang, C., Wang, R., Xu, P., Cheng, M., Huang, C., Wu, H., Qin, L., 2016. Synthesis of surface molecular imprinted TiO_2/graphene photocatalyst and its highly efficient photocatalytic degradation of target pollutant under visible light irradiation. Appl. Surf. Sci. 390, 368–376.

Lai, C., Zhang, M., Li, B., Huang, D., Zeng, G., Qin, L., Liu, X., Yi, H., Cheng, M., Li, L., Chen, Z., Chen, L., 2019a. Fabrication of CuS/$BiVO_4$ (040) binary heterojunction photocatalysts with enhanced photocatalytic activity for Ciprofloxacin degradation and mechanism insight. Chem. Eng. J. 358, 891–902.

Lair, A., Ferronato, C., Chovelon, J.M., Herrmann, J.M., 2008. Naphthalene degradation in water by heterogeneous photocatalysis: an investigation of the influence of inorganic anions. J. Photochem. Photobio. A 193 (2–3), 193–203.

Li, B., Lai, C., Zeng, G., Qin, L., Yi, H., Huang, D., Zhou, C., Liu, X., Cheng, M., Xu, P., Zhang, C., Huang, F., Liu, S., 2018. Facile hydrothermal synthesis of Z-scheme $Bi_2Fe_4O_9/Bi_2WO_6$ heterojunction photocatalyst with enhanced visible light photocatalytic activity. ACS Appl. Mater. Interfaces 10 (22), 18824–18836.

Li, B., Yang, L., Wang, C., Zhang, Q., Liu, Q., Li, Y., Xiao, R., 2017a. Adsorption of Cd(II) from aqueous solutions by rape straw biochar derived from different modification processes. Chemosphere 175, 332–340.

Li, K., Zhao, Y., Janik, M.J., Song, C., Guo, X., 2017b. Facile preparation of magnetic mesoporous Fe_3O_4/C/Cu composites as high performance Fenton-like catalysts. Appl. Surf. Sci. 396, 1383–1392.

Liu, M., Wu, X., Liu, S., Gao, Y., Chen, Z., Ma, Y., Ran, R., Weng, D., 2017. Study of Ag/CeO_2 catalysts for naphthalene oxidation: balancing the oxygen availability and oxygen regeneration capacity. Appl. Catal. B: Environ. 219, 231–240.

Liu, Y., Liu, Z., Huang, D., Cheng, M., Zeng, G., Lai, C., Zhang, C., Zhou, C., Wang, W., Jiang, D., Wang, H., Shao, B., 2019. Metal or metal-containing nanoparticle@MOF nanocomposites as a promising type of photocatalyst. Coord. Chem. Rev. 388, 63–78.

Nguyen, T.D., Phan, N.H., Do, M.H., Ngo, K.T., 2011. Magnetic Fe_2MO_4 (M:Fe, Mn) activated carbons: fabrication, characterization and heterogeneous Fenton oxidation of methyl orange. J. Hazard. Mater. 185 (2–3), 653–661.

Nogueira, R.F., Oliveira, M.C., Paterlini, W.C., 2005. Simple and fast spectrophotometric determination of H_2O_2 in photo-Fenton reactions using metavanadate. Talanta 66 (1), 86–91.

Ouyang, D., Yan, J., Qian, L., Chen, Y., Han, L., Su, A., Zhang, W., Ni, H., Chen, M., 2017. Degradation of 1,4-dioxane by biochar supported nano magnetite particles activating persulfate. Chemosphere 184, 609–617.

Qin, L., Huang, D., Xu, P., Zeng, G., Lai, C., Fu, Y., Yi, H., Li, B., Zhang, C., Cheng, M., Zhou, C., Wen, X., 2019. In-situ deposition of gold nanoparticles onto polydopamine-decorated g-C_3N_4 for highly efficient reduction of nitroaromatics in environmental water purification. J. Colloid Interface Sci. 534, 357–369.

Qin, Y., Li, G., Gao, Y., Zhang, L., Ok, Y.S., An, T., 2018. Persistent free radicals in carbon-based materials on transformation of refractory organic contaminants (ROCs) in water: a critical review. Water Res. 137, 130–143.

Ruales-Lonfat, C., Barona, J.F., Sienkiewicz, A., Bensimon, M., Vélez-Colmenares, J., Benítez, N., Pulgarín, C., 2015. Iron oxides semiconductors are efficients for solar water disinfection: a comparison with photo-Fenton processes at neutral pH. Appl. Catal. B: Environ. 166–167, 497–508.

Sekar, A.D., Muthukumar, H., Chandrasekaran, N.I., Matheswaran, M., 2018. Photocatalytic degradation of naphthalene using calcined FeZnO/PVA nanofibers. Chemosphere 205, 610–617.

Tang, J., Huang, Y., Gong, Y., Lyu, H., Wang, Q., Ma, J., 2016. Preparation of a novel graphene oxide/Fe-Mn composite and its application for aqueous Hg(II) removal. J. Hazard. Mater. 316, 151–158.

Wang, G., Zhao, D., Kou, F., Ouyang, Q., Chen, J., Fang, Z., 2018. Removal of norfloxacin by surface Fenton system ($MnFe_2O_4/H_2O_2$): kinetics, mechanism and degradation pathway. Chem. Eng. J. 351, 747–755.

Wan, Z., Wang, J., 2017a. Degradation of sulfamethazine antibiotics using Fe_3O_4-Mn_3O_4 nanocomposite as a Fenton-like catalyst. J. Chem. Technol. Biotechnol. 92 (4), 874–883.

Wan, Z., Wang, J., 2017b. Degradation of sulfamethazine using Fe_3O_4-Mn_3O_4/reduced graphene oxide hybrid as Fenton-like catalyst. J. Hazard. Mater. 324, 653–664.

Wu, S., He, H., Inthapanya, X., Yang, C., Lu, L., Zeng, G., Han, Z., 2017. Role of biochar on composting of organic wastes and remediation of contaminated soils—a review. Environ. Sci. Pollut. Res. 24 (20), 1–18.

Xie, Y.C., Tang, Y.Q., 1990. Spontaneous monolayer dispersion of oxides and salts onto surfaces of supports: applications to heterogeneous catalysis. Adv. Catal. 37, 1–43.

Xue, Y., Sui, Q., Brusseau, M.L., Zhang, X., Qiu, Z., Lyu, S., 2018. Insight on the generation of reactive oxygen species in the CaO_2/Fe(II) Fenton system and the hydroxyl radical advancing strategy. Chem. Eng. J. 353, 657–665.

Yang, F., Zhang, S., Li, H., Li, S., Cheng, K., Li, J.S., Tsang, D.C.W., 2018a. Corn straw-derived biochar impregnated with α-FeOOH nanorods for highly effective copper removal. Chem. Eng. J. 348, 191–201.

Yang, X., Cai, H., Bao, M., Yu, J., Lu, J., Li, Y., 2018b. Insight into the highly efficient degradation of PAHs in water over graphene oxide/Ag_3PO_4 composites under visible light irradiation. Chem. Eng. J. 334, 355–376.

Yi, H., Yan, M., Huang, D., Zeng, G., Lai, C., Li, M., Huo, X., Qin, L., Liu, S., Liu, X., Li, B., Wang, H., Shen, M., Fu, Y., Guo, X., 2019. Synergistic effect of artificial enzyme and 2D nano-structured Bi_2WO_6 for eco-friendly and efficient biomimetic photocatalysis. Appl. Catal. B: Environ. 250, 52–62.

Zhang, C., Wang, W., Duan, A., Zeng, G., Huang, D., Lai, C., Tan, X., Cheng, M., Wang, R., Zhou, C., Xiong, W., Yang, Y., 2019. Adsorption behavior of engineered carbons and carbon nanomaterials for metal endocrine disruptors: experiments and theoretical calculation. Chemosphere 222, 184–194.

Zhao, J., Zhao, Z., Li, N., Nan, J., Yu, R., Du, J., 2018a. Visible-light-driven photocatalytic degradation of ciprofloxacin by a ternary $Mn_2O_3/Mn_3O_4/MnO_2$ valence state heterojunction. Chem. Eng. J. 353, 805–813.

Zhao, N., Yin, Z., Liu, F., Zhang, M., Lv, Y., Hao, Z., Pan, G., Zhang, J., 2018b. Environmentally persistent free radicals mediated removal of Cr(VI) from highly saline water by corn straw biochars. Bioresour. Technol. 260, 294–301.

Zhong, Y., Liang, X., He, Z., Tan, W., Zhu, J., Yuan, P., Zhu, R., He, H., 2014. The constraints of transition metal substitutions (Ti, Cr, Mn, Co and Ni) in magnetite on its catalytic activity in heterogeneous Fenton and UV/Fenton reaction: from the perspective of hydroxyl radical generation. Appl. Catal. B: Environ. 150–151, 612–618.

Zhong, Y., Liang, X., Zhong, Y., Zhu, J., Zhu, S., Yuan, P., He, H., Zhang, J., 2012. Heterogeneous UV/Fenton degradation of TBBPA catalyzed by titanomagnetite: catalyst characterization, performance and degradation products. Water Res. 46 (15), 4633–4644.

Zhou, X., Lai, C., Huang, D., Zeng, G., Chen, L., Qin, L., Xu, P., Cheng, M., Huang, C., Zhang, C., Zhou, C., 2018. Preparation of water-compatible molecularly imprinted thiol-functionalized activated titanium dioxide: selective adsorption and efficient photodegradation of 2, 4-dinitrophenol in aqueous solution. J. Hazard. Mater. 346, 113–123.

Zhou, Y., Xiao, B., Liu, S.Q., Meng, Z., Chen, Z.G., Zou, C.Y., Liu, C.B., Chen, F., Zhou, X., 2016. Photo-Fenton degradation of ammonia via a manganese–iron double-active component catalyst of graphene–manganese ferrite under visible light. Chem. Eng. J. 283, 266–275.